Effect of Catalyst Structure on Growth and Reactivity of Carbon Nanofibers over Ni/MgAl2O4

ARTICLE *in* INDUSTRIAL & ENGINEERING CHEMISTRY RESEARCH · JUNE 2013

Impact Factor: 2.59 · DOI: 10.1021/ie400688y

4 AUTHORS, INCLUDING:

Xiaoliang Yan
Zhejiang University of Media and Communicat…
16 PUBLICATIONS **102** CITATIONS
SEE PROFILE

Chang-Jun Liu
Tianjin University
153 PUBLICATIONS **3,424** CITATIONS
SEE PROFILE

I&EC research
Industrial & Engineering Chemistry Research

Article

pubs.acs.org/IECR

Effect of Catalyst Structure on Growth and Reactivity of Carbon Nanofibers over Ni/$MgAl_2O_4$

Binran Zhao, Xiaoliang Yan, You Zhou, and Chang-jun Liu*

Advanced Nanotechnology Center, School of Chemical Engineering and Technology, Tianjin University, Tianjin 300072, China

Supporting Information

ABSTRACT: The structure of Ni catalyst has a significant effect on the growth and reactivity of carbon nanofibers (CNFs) formed from methane decomposition. We present here a detailed study on this structure effect with Ni/$MgAl_2O_4$ as model catalyst. Different catalyst structures were obtained via dielectric barrier discharge (DBD) plasma and thermal decomposition. For the thermal decomposed catalyst, a complex combination of microfacets presents with a higher content of defects. A diffusion interfacial region is formed due to the migration of Ni atoms into the support. However, a higher concentration of close-packed plane is observed for the DBD decomposed catalyst with less defects and a clean interface between Ni particle and support. The CNFs over the DBD decomposed sample show smaller diameter and narrower distribution with a smaller slope of graphene layers but enhanced activity toward O_2 and CO_2, indicating better coke resistance for methane conversion.

1. INTRODUCTION

Methane is the principal component of natural gas, biogas, coal-bed methane, gas hydrate, and shale gas. Methane conversion has been industrially applied for syngas ($CO + H_2$) production via steam reforming. It has been extensively exploited for the possible production of CO_2-free hydrogen, carbon nanotube, carbon nanofiber, carbon black, aromatics, ethylene, methanol, acetic acid, clean energy (via methane combustion), and others. With the very recent development of shale gas production, methane conversion attracts even more attention.

Methane conversion is normally performed via catalysts at elevated temperatures (because of the inertness of the methane molecule). Nickel is a very popular catalyst for methane conversion because of its plentiful resources. One normally disperses nickel onto various supporting materials like alumina, $MgAl_2O_4$ and others. The reactions with supported Ni catalysts include steam reforming,[1,2] CO_2 reforming,[3−5] partial oxidation,[6] and methane decomposition[7−9] (toward CO_2-free hydrogen or carbon nanostructured materials). Extensive studies have been conducted to understand the mechanism of methane conversion over the Ni catalysts. It has been confirmed that the reaction condition, catalyst size, and structure have a significant influence on methane conversion.[10,11] Especially, the Ni catalyst thermodynamically tends to form carbon during methane conversion. The size and structure of the catalyst also have a significant effect on the carbon formation. Different catalyst structures result in totally different carbon nanostructured materials. As reported by Chen et al.,[9] small Ni crystals yield a low growth rate and fast deactivation and thus a low final yield of carbon nanofibers (CNFs). Takenaka et al.[12] found that the reaction temperature controls the diameter and graphitic order of carbon nanofibers. Martinez-Latorre et al.[13] also reported that the growth temperature can control the primary structure of CNFs, either rolled graphitic planes parallel to the axis (multiwall carbon nanotubes) or graphitic planes forming an angle with respect to the axis (fishbone type). For the methane conversions with carbon not as the objective product, a serious carbon formation will induce a deactivation of the catalyst.[10] The reactivity of the formed carbon has a significant influence not only on the yield but also on the production cost for methane conversion. For example, a high steam-to-carbon feed ratio has been used in the industrial syngas production via steam reforming of methane in order to limit the carbon formation. This high ratio obviously leads to high production cost with high energy input. The Ni catalyst with a good balance between carbon formation and further gasification must be excellent for methane conversion. To do so, one would design a catalyst with low carbon formation rate or make a catalyst that can generate more carbon species with improved reactivity for further gasification reactions (with steam, CO_2, or oxygen).[10] Many efforts have been conducted toward this goal via the studies of the promoters, supporting materials, preparation conditions, and Ni precursors. Theoretical studies have also demonstrated that Ni(111) has a low methane dissociation activity, compared to Ni(100) and others.[14] However, few experimental works have been conducted on the effect of the crystal structure of nickel itself. The reason for it is that the supported Ni catalysts are normally prepared by thermal calcination. The calcination thermally always leads to a formation of Ni polycrystalline nanoparticles. It is not easy to do a structure control of the Ni catalysts. In this regard, several groups confirmed that the decomposition of Ni precursors under the influence of cold plasmas leads to catalysts with enhanced coke resistance for methane conversion.[2,10,15−19] The Ni catalysts made by plasma decomposition show smaller size and enhanced Ni-support interaction. Yan et al.[20,21] demonstrated that only Ni(111) can be observed from the TEM image of the plasma-made catalysts. The energetic electrons and active oxygen species within cold plasmas have been considered to be responsible for the

Received: March 2, 2013
Revised: May 9, 2013
Accepted: May 24, 2013
Published: May 24, 2013

improved properties. However, no study has been conducted in detail for the plasma effect on the Ni catalyst structure for methane conversion.

In this work, we attempt to investigate the growth and reactivity of carbon nanofibers over Ni/$MgAl_2O_4$ catalysts prepared by dielectric-barrier discharge (DBD) plasma decomposition. The catalyst prepared by the plasma decomposition shows a very different structure compared to the catalyst prepared by the thermal decomposition. This provides us an excellent model catalyst to better understand the effect of the catalyst structure. DBD plasma is one of the cold plasma phenomena. It has been used for the decomposition of metal precursors,[20,21] fabrication of oxide,[22,23] and template removal.[24,25] A typical advantage of the DBD plasma is that it can be initiated at room temperature and operated at low temperature (less than 200 °C) under atmospheric pressure with air directly as the plasma generating gas.

2. EXPERIMENTAL SECTION

2.1. Catalyst Preparation. The Ni/$MgAl_2O_4$ catalyst was prepared by the incipient wetness impregnation method. The $MgAl_2O_4$ powder was obtained through the calcination of hydrotalcite (Sasol) at 900 °C for 16 h (S_{BET} = 90−100 $m^2\ g^{-1}$). It was then impregnated with an aqueous solution of nickel nitrate for about 12 h. The obtained sample was dried at 110 °C for another 12 h. The dried sample (assigned as Ni/$MgAl_2O_4$−IM) was divided into two parts for further decomposition. One part was calcined thermally at 500 °C for 4 h. The other part was treated by the DBD plasma. The color of the sample was changed into dark-gray gradually during the DBD decomposition (Supporting Information, Figure S1). This means nickel nitrate is effectively decomposed by the DBD plasma. The same conclusion can be made by thermogravimetry (shown in Supporting Information, Figure S2). The catalysts obtained by plasma and thermal decomposition are denoted as Ni/$MgAl_2O_4$−DBD and Ni/$MgAl_2O_4$−Cal, respectively. The loading amount of Ni is 10 wt % in this work.

The DBD setup has been previously described in detail.[20−25] Briefly, two steel plate electrodes are covered by quartz plates with a thickness of 2.5 mm. The diameter of the quartz plates and the steel plates is 90 and 50 mm, respectively. The width of the discharge gap, that is, the distance between the two quartz plates, is 8 mm. Air was directly employed as the plasma forming gas. The powder sample (0.5 g) was placed on the lower quartz plate. A high voltage generator (CTP-2000K; Corona Laboratory, Nanjing, China), which could supply a voltage from 0 to 30 kV with a sinusoidal waveform, was used to generate the DBD plasma. The average voltage was 14 kV with a sinusoidal waveform at a frequency of about 22 kHz. The input power was 200 W.

2.2. Characterization. The X-ray powder diffraction (XRD) patterns of the samples were recorded on a Rigaku D/Max-2500 diffractometer at a scanning speed of 4°/min over the 2θ range of 10−70°. The diffractometer was equipped with a Ni-filtered Cu Kα radiation source (λ = 1.54056 Å). The phase identification was made by comparison to the Joint Committee on Powder Diffraction Standards (JCPDSs).

TEM analyses were performed on a Philips Tecnai G^2 F20 system operated at 200 kV. The samples were suspended into ethanol and dispersed ultrasonically for 15 min. A drop of the suspension was deposited on a copper grid coated with carbon.

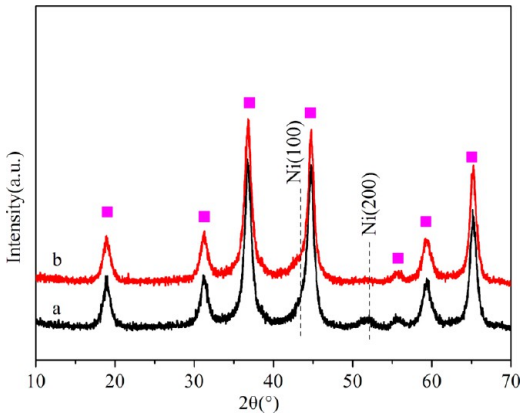

Figure 1. XRD patterns of Ni/$MgAl_2O_4$−Cal (a) and Ni/$MgAl_2O_4$−DBD (b) after H_2 reduction; ■, $MgAl_2O_4$.

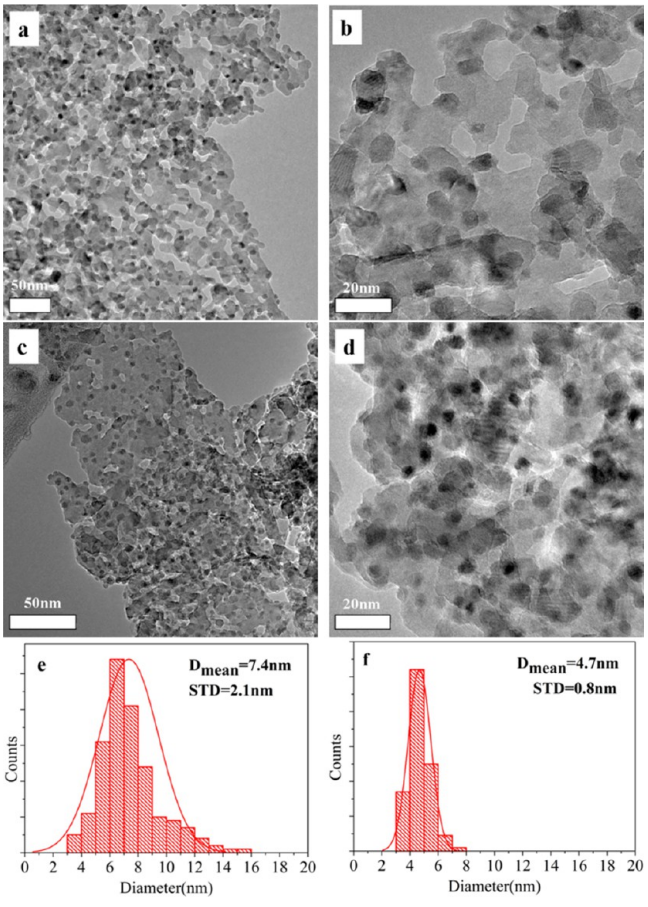

Figure 2. TEM images and the corresponding particle size distributions of Ni/$MgAl_2O_4$−Cal (a, b, e) and Ni/$MgAl_2O_4$−DBD (c, d, f) after H_2 reduction.

2.3. Methane Decomposition. Methane decomposition was carried out in a quartz-tube fixed-bed reactor horizontally placed in a furnace under atmospheric pressure. The catalyst (30 mg) was first heated to 120 °C in Ar. Hydrogen was then switched on and the heating was going on until 700 °C. The reduction was maintained at 700 °C for 1 h. After the reduction, the temperature was decreased to the reaction temperature, and the sample was purged with Ar at the same temperature for 1 h. A mixture of CH_4 (>99.999%) and Ar (>99.999%) at 30 cm^3/min with a molar ratio of 1:2 was

dx.doi.org/10.1021/ie400688y | Ind. Eng. Chem. Res. 2013, 52, 8182−8188

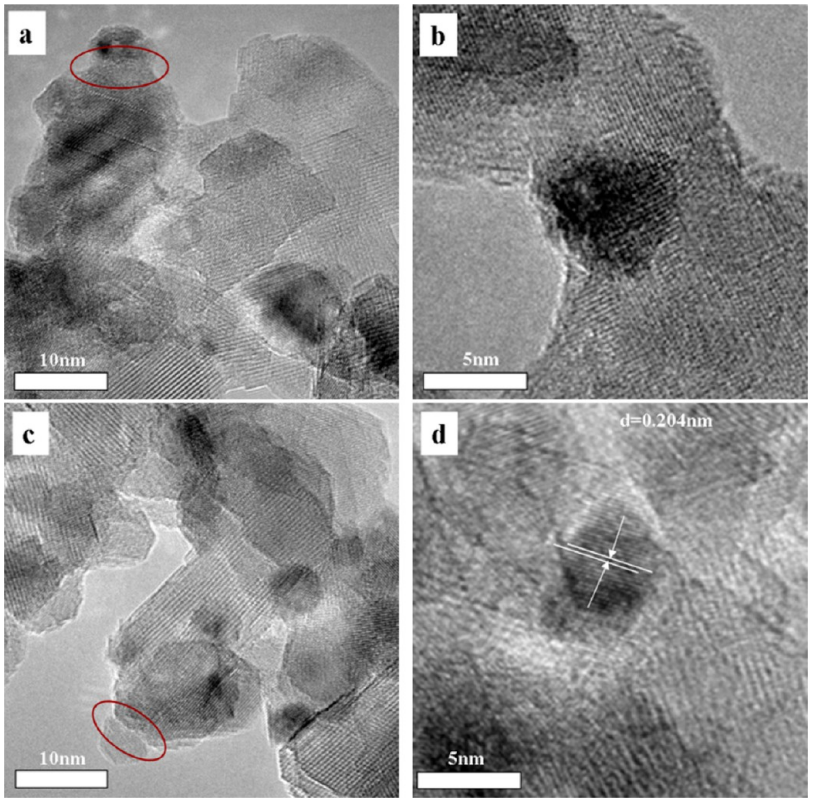

Figure 3. High resolution TEM images of Ni/$MgAl_2O_4$−Cal (a, b) and Ni/$MgAl_2O_4$−DBD (c, d) after H_2 reduction.

introduced into the microreactor by mass flow controllers. The reaction lasted for 2 h. The gas residue was analyzed online by a gas chromatograph (GC, Agilent 6890), equipped with a thermal conductivity detector (TCD) and a Porapak Q column.

2.4. Temperature-Programmed Reactions. Before the temperature-programmed reactions, methane decomposition was conducted as described in section 2.3 at 500 °C for 10 min. During the temperature-programmed oxidation (TPO), the sample was heated in flowing 3% O_2/He at 30 cm^3/min over the temperature range 50−1000 °C at a heating rate of 10 °C/min. The CO_2 (m/z = 44) signals were continuously recorded by an online quadrupole mass spectrometer (GSD301, Ommistar).

During the temperature−programmed reaction with CO_2 ($TPCO_2$) analysis, the catalyst sample was heated within the temperature range 50−1000 °C at a heating rate of 10 °C/min. A gaseous mixture of CO_2 and argon (Ar) with a volume ratio of 1:2 was fed into the reactor at a flow rate of 30 cm^3/min. The CO (m/z = 28) signals were continuously recorded by the same mass spectrometer used for the above TPO analysis.

3. RESULTS AND DISCUSSION

3.1. Characterization of the Catalysts. *3.1.1. XRD.* The XRD patterns of fresh catalysts are presented in Figure 1. For all the cases, diffraction peaks attributed to the support $MgAl_2O_4$ (2θ = 19.03°, 31.3°, 36.8°, 44.8°, 55.6°, 59.4° and 65.2°, JCPDS-21-1152) and Ni (2θ = 44.5°, 51.8°, JCPDS-04-0850) are detected. Because of the overlap of the peaks of Ni(111) and $MgAl_2O_4$(400), we analyze the peaks assigned to Ni(200) here. The intensity of Ni(200) of Ni/$MgAl_2O_4$−DBD is much lower than that of the Ni/$MgAl_2O_4$−Cal, which indicates that smaller Ni particles are fabricated via the DBD decomposition.

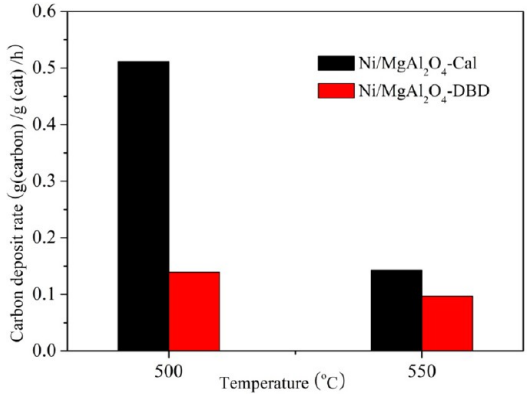

Figure 4. Carbon deposition rate of CH_4 decomposition for Ni/$MgAl_2O_4$−Cal and Ni/$MgAl_2O_4$−DBD at 500 and 550 °C.

3.1.2. TEM. Figure 2 shows the TEM images and the corresponding particle size distributions of the reduced catalysts. The particle diameters are 7.4 ± 2.1 nm and 4.7 ± 0.8 nm for the reduced Ni/$MgAl_2O_4$−Cal and Ni/$MgAl_2O_4$−DBD, respectively. Compared to the large and uneven Ni particles for the thermal decomposed sample, homogeneously higher dispersed Ni particles are obtained by the DBD plasma decomposition method, which has been confirmed by XRD. Besides the particle size, the roundness of the Ni particles is also better for the latter catalyst according to Figure 2b,d.

The metal−support interface is indistinct for the reduced Ni/$MgAl_2O_4$−Cal sample, shown in Figure 3a. As reported by Zou et al.[26] and Yan et al.,[21,22] the nickel atoms can diffuse into the bulk of the support due to the thermal calcination. So a diffused interfacial region is formed, instead of the metal−support interface. By contrast, for the reduced Ni/$MgAl_2O_4$−DBD,

dx.doi.org/10.1021/ie400688y | Ind. Eng. Chem. Res. 2013, 52, 8182−8188

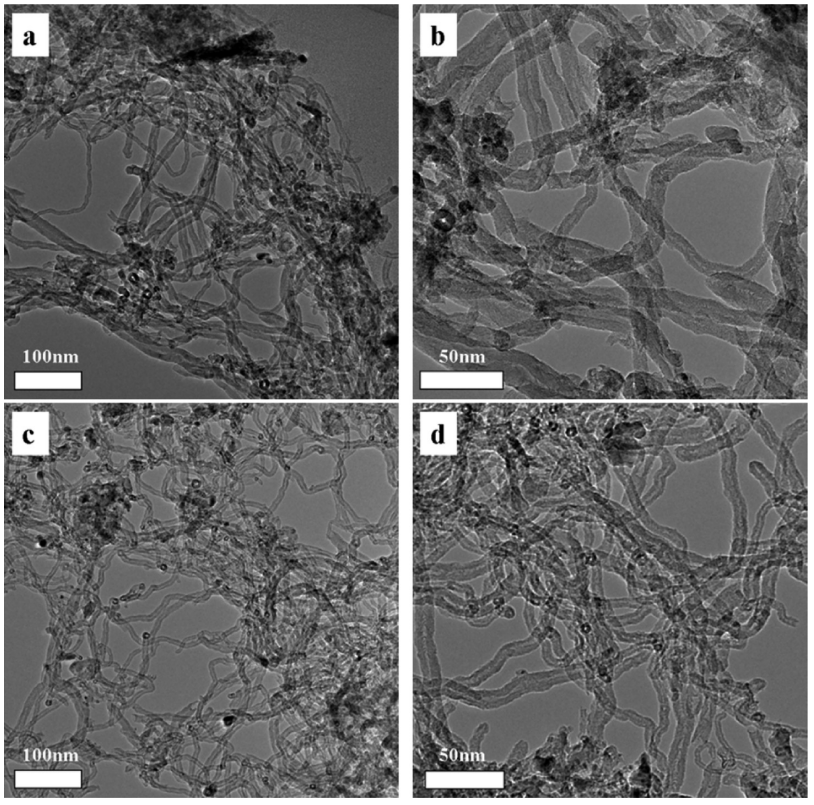

Figure 5. TEM images of CNFs growing over Ni/$MgAl_2O_4$−Cal (a, b) and Ni/$MgAl_2O_4$−DBD (c, d) at 500 °C.

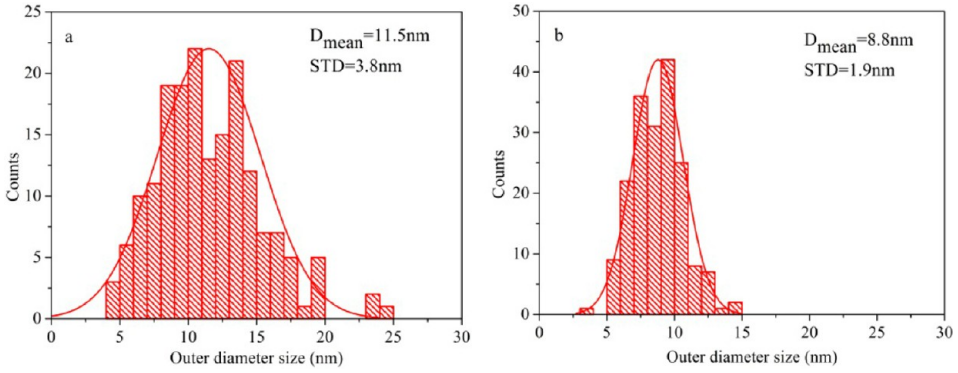

Figure 6. Outer diameter distributions of CNFs growing over Ni/$MgAl_2O_4$−Cal (a) and Ni/$MgAl_2O_4$−DBD (b) at 500 °C.

a clean and direct interface is observed without the diffused interfacial region (Figure 3c). In addition, no specific crystallographic plane orientation is observed for Ni/$MgAl_2O_4$−Cal (Figure 3b). This particle surface can be considered as a complex combination of microfacets presenting a high concentration of edges, corners, and various types of surface defects. However, well-defined lattice fringes of the Ni (111) plane are clearly observed for Ni/$MgAl_2O_4$−DBD, as shown in Figure 3d. The perfect surface with less defect sites is thus obtained by DBD plasma decomposition with respect to that by thermal decompotion.

3.2. Activity of Catalysts. Methane decomposition was conducted over Ni/$MgAl_2O_4$−Cal and Ni/$MgAl_2O_4$−DBD samples. For both catalysts, only H_2 is detected as the gaseous product. The methane conversion is high at the initial step of the reaction. It decreases gradually with time on stream. A lower initial activity is observed for the DBD decomposed sample. The catalyst is deactivated in 60 min. Whereas the calcined sample shows higher activity and lower deactivated rate (Supporting Information, Figure S3), Figure 4 shows the carbon deposition rate with time on stream at 500 and 550 °C over the Ni/$MgAl_2O_4$−Cal and Ni/$MgAl_2O_4$−DBD samples. At 500 °C, the carbon deposition rate of Ni/$MgAl_2O_4$−Cal is 0.511 g(carbon)/g(cat)/h, which is more than 3 times higher than that of Ni/$MgAl_2O_4$−DBD. A similar result is obtained at 550 °C.

The result is probably caused by two reasons. First, it is well-known that the decomposition of methane is structure sensitive, with higher activation energy over close packed planes (i.e., high coordinated sites, such as Ni(111)) than that over defect sites or open planes (i.e., low coordinated sites, such as Ni (100)).[16,21,26,27] Ni (111) plane observed in TEM image of Ni/$MgAl_2O_4$−DBD goes against methane decomposition, resulting in the lower activity and lower carbon deposition rate. Second, the smaller particle size also contributes to the result. Chen et al.[9] reported that the carbon growth rate reduces and deactivation rate increases as the particle size decreases when the Ni particles is smaller than

dx.doi.org/10.1021/ie400688y | Ind. Eng. Chem. Res. 2013, 52, 8182−8188

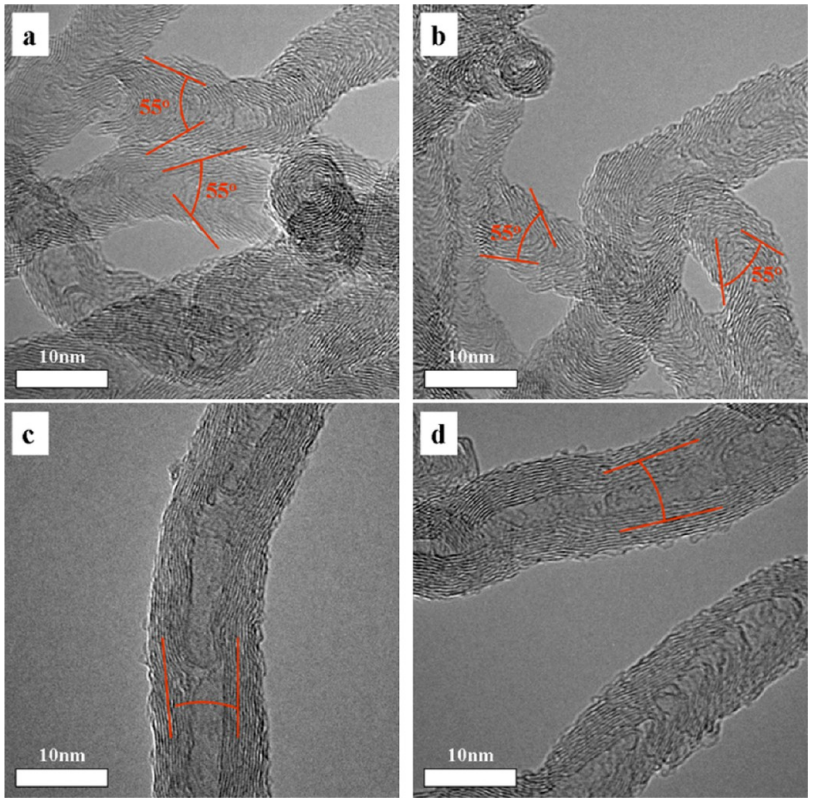

Figure 7. High resolution TEM images of CNFs growing on Ni/$MgAl_2O_4$−Cal (a, b) and Ni/$MgAl_2O_4$−DBD (c, d) at 500 °C.

34 nm. Therefore the lower initial activity and carbon deposition rate for Ni/$MgAl_2O_4$−DBD can be attributed to the relatively perfect surface and smaller particles. This indicates that Ni/$MgAl_2O_4$−DBD has a better coke resistant property for methane conversion.

3.3. Carbon Nanofiber Characterization. *3.3.1. TEM.* Figure 5 exhibits the TEM images of the CNFs produced over the two catalysts. The typical CNF structure, cylindrical hollow shape, is observed for both samples. The diameter of the CNFs produced over Ni/$MgAl_2O_4$−Cal is in the range from 4 to 25 nm with an average diameter of 11.5 ± 3.8 nm. In contrast, the DBD treated catalyst gives a narrower CNF diameter size distribution with a smaller average diameter of 8.8 ± 1.9 nm, as shown in Figure 6. From the TEM results, smaller Ni particles are also observed for the reduced DBD treated catalyst with high dispersion. Obviously, the size of the Ni catalyst can be used to control the diameter of CNFs thanks to the diameter coincidence of Ni particles and CNFs.[28,29] In addition, the produced CNFs over Ni/$MgAl_2O_4$−DBD are smoother with fewer nodes along the nanofibers. This is probably due to the uniform morphology of Ni particles and well-defined lattice fringes of Ni surface. Here the "base-growth" mechanism is proposed because Ni particles are seldom observed on the tips of both CNFs.

The high resolution TEM images of the CNFs presented in Figure 7 show the difference of the slope of graphene layers, that is, the angle α between the graphene layers and the orientation of CNF growth. The value of α is 55° for the CNFs produced over Ni/$MgAl_2O_4$−Cal, whereas it is near 0° for that over Ni/$MgAl_2O_4$−DBD. The slope of graphene layers is the duplication of the interface between the Ni particle and the formed carbon. It is greatly affected by the relationship of carbon deposition rate and carbon diffusion rate on metal Ni surface. As analyzed in section 3.2, the Ni surface is a complex combination of microfacets for Ni/$MgAl_2O_4$−Cal and close-packed plane Ni(111) for Ni/$MgAl_2O_4$−DBD. Hofmann et al.[30] has reported the adsorbed C on the Ni(111) is bonded to 3 Ni atoms, and the barrier for carbon diffusion on the Ni(111) surface is 0.4 eV. Whereas, the C atom is bonded to 5 Ni, and the barrier is 1.9 eV on the Ni(100),[30] the carbon diffusion is more difficult for Ni/$MgAl_2O_4$−Cal than for Ni/$MgAl_2O_4$−DBD. And methane is expected to be dissociated from all directions of the Ni particles for the rough surfaces with higher concentration of defect sites and a complex combination of microfacets for Ni/$MgAl_2O_4$−Cal,[16,31] shown in Figure 8a.

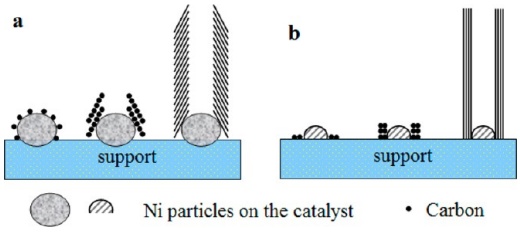

Figure 8. Schematic representation of CNF growth over on Ni/$MgAl_2O_4$−Cal (a) and Ni/$MgAl_2O_4$−DBD (b).

Therefore the carbon deposition rate over Ni/$MgAl_2O_4$−Cal is much higher. The slower surface diffusion is probably blocked by the high carbon coverage. As a result, the graphene layers arrange along the surface of the Ni particles and eventually form the CNFs with larger α value. For Ni/$MgAl_2O_4$−DBD, the carbon deposition rate is much lower and the surface carbon diffuses rapidly along Ni(111) to the Ni/support interface and finally forms the CNFs with smaller α value as shown in Figure 8b.

dx.doi.org/10.1021/ie400688y | Ind. Eng. Chem. Res. 2013, 52, 8182−8188

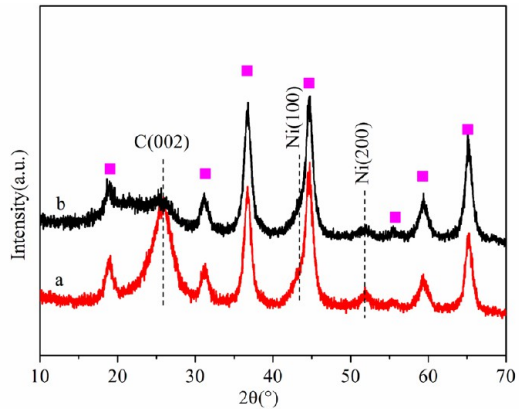

Figure 9. XRD patterns of the used $Ni/MgAl_2O_4$–Cal (a) and $Ni/MgAl_2O_4$–DBD (b) after reaction at 500 °C; ■, $MgAl_2O_4$.

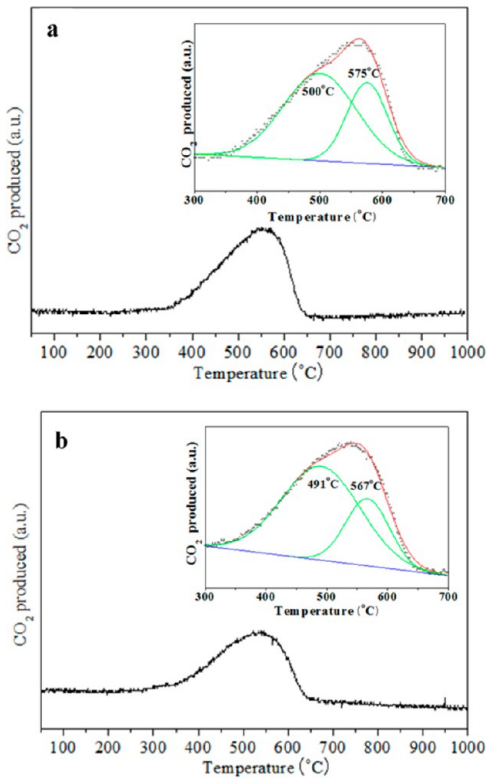

Figure 10. TPO profiles of $Ni/MgAl_2O_4$–Cal (a) and $Ni/MgAl_2O_4$–DBD (b).

3.3.2. XRD. Figure 9 shows the XRD patterns of the used catalysts. After methane decomposition, Ni particles and the support are kept intact. However, an unambiguous peak assigned to graphite carbon (002) appears at $2\theta = 26°$. The higher peak for $Ni/MgAl_2O_4$–Cal suggests that the carbon formed on the surface of $Ni/MgAl_2O_4$–Cal is more ordered than that of $Ni/MgAl_2O_4$–DBD, which indicates that this carbon is inactive.

3.3.3. The activity of the CNFs. For CO_2 reforming and partial oxidation of methane, methane decomposition is one pathway of coke formation. The methane-derived carbon can be gasified by O_2 or CO_2. If the gasification of carbon is slower, it will deposit and deactivate the catalyst. To study the activity of the obtained CNFs, the TPO and $TPCO_2$ experiments are conducted.

Figure 10 shows the TPO results of $Ni/MgAl_2O_4$–Cal and $Ni/MgAl_2O_4$–DBD. According to the oxidized temperature, two kinds of carbon are generated for both catalysts, which are defined as C_{LT} and C_{HT} here. The C_{LT} is oxidized at around 500 °C, and the C_{HT} at 570 °C. For $Ni/MgAl_2O_4$–DBD, the oxidized temperatures of C_{LT} and C_{HT} are lower than those for $Ni/MgAl_2O_4$–Cal. The ratio (obtained from the peak areas) of C_{LT} and C_{HT} is 1.95:1 for $Ni/MgAl_2O_4$–Cal and 2.50:1 for $Ni/MgAl_2O_4$–DBD. More C_{LT} indicates that the carbon formed over $Ni/MgAl_2O_4$–DBD is more active than that over $MgAl_2O_4$–Cal. Similar conclusions can be made from the $TPCO_2$ study (Figure 11). The reaction temperature between

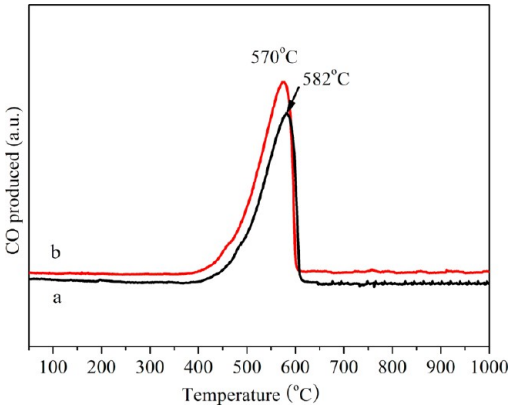

Figure 11. $TPCO_2$ profiles of $Ni/MgAl_2O_4$–Cal (a) and $Ni/MgAl_2O_4$–DBD (b).

carbon and CO_2 is lower for $Ni/MgAl_2O_4$–DBD, and the carbon deposition rate (Figure 4) indicates that more carbon is generated over $Ni/MgAl_2O_4$–Cal. However, according to the peak area of $TPCO_2$, less CO is generated for this catalyst. This means that some carbon over $Ni/MgAl_2O_4$–Cal is inactive toward CO_2 even though the temperature is as high as 1000 °C. After the $TPCO_2$ reaction, besides the light green particles, some dark ones are also observed for $Ni/MgAl_2O_4$–Cal. The dark ones are probably caused by the residual carbon which does not react with CO_2 (Supporting Information, Figure S4). Whereas for $Ni/MgAl_2O_4$–DBD, only light green particles are observed, this means that the formed carbon is completely gasified by CO_2. Thus the carbon produced over the DBD plasma decomposed catalyst is more active than that over the thermal decomposed one, which is in accordance with the XRD results.

4. CONCLUSIONS

The $Ni/MgAl_2O_4$ catalyst prepared by DBD plasma shows higher dispersion of Ni with narrower size distribution compared to the thermal decomposed catalyst. The plasma decomposed catalyst has less defect sites with more Ni(111), and the interface of Ni and the support for $Ni/MgAl_2O_4$–DBD is clean and direct without the diffusion interfacial region observed for $Ni/MgAl_2O_4$–Cal. These factors lead to a lower carbon deposition rate of methane decomposition over $Ni/MgAl_2O_4$–DBD. The obtained CNFs over DBD decomposed catalyst have a smaller diameter and narrower diameter size distribution than those over the thermal decomposed sample. The CNFs produced over $Ni/MgAl_2O_4$–DBD show a different slope of graphene layers but enhanced activity toward O_2 and CO_2, indicating the potential of better coke resistance for CO_2 reforming and partial oxidation of methane.

dx.doi.org/10.1021/ie400688y | Ind. Eng. Chem. Res. 2013, 52, 8182–8188

■ ASSOCIATED CONTENT

Supporting Information

The analysis of decomposed degree, activity of the catalysts and the image of catalysts after $TPCO_2$ reaction. This material is available free of charge via the Internet at http://pubs.acs.org.

■ AUTHOR INFORMATION

Corresponding Author

*Fax: +86 22 27406490. E-mail: ughg_cjl@yahoo.com.

Notes

The authors declare no competing financial interest.

■ ACKNOWLEDGMENTS

The support from the National Natural Science Foundation of China (under Contract No. 20990223) is greatly appreciated.

■ REFERENCES

(1) Bang, Y.; Lee, J.; Han, S. J.; Seo, J. G.; Youn, M. H.; Song, J. H.; Song, I. K. Hydrogen production by steam reforming of liquefied natural gas (LNG) over mesoporous nickel-alumina xerogel catalysts prepared by a single-step carbon-templating sol-gel method. *Intern. J. Hydrogen Energy* **2012**, *37*, 11208.

(2) Guo, X. Y.; Sun, Y. L.; Yu, Y.; Zhu, X. L.; Liu, C. J. Carbon formation and steam reforming of methane on silica supported nickel catalysts. *Catal. Commun.* **2012**, *19*, 61.

(3) Centi, G.; Perathoner, S. Opportunities and prospects in the chemical recycling of carbon dioxide to fuels. *Catal. Today* **2009**, *148*, 191.

(4) Tu, X.; Whitehead, J. C. Plasma-catalytic dry reforming of methane in an atmospheric dielectric barrier discharge: Understanding the synergistic effect at low temperature. *Appl. Catal., B* **2012**, *125*, 439.

(5) Xu, L.; Song, H.; Chou, L. Carbon dioxide reforming of methane over ordered mesoporous NiO−MgO−Al_2O_3 composite oxides. *Appl. Catal., B* **2011**, *108*, 177.

(6) Liu, T.; Snyder, C.; Veser, G. Catalytic partial oxidation of methane: Is a distinction between direct and indirect reaction mechanism meaningful? *Ind. Eng. Chem. Res.* **2007**, *46*, 9045.

(7) Gonzalez, I.; de Jesus, J. C.; Canizales, E.; Delgado, B.; Urbina, C. Comparison of the surface state of Ni nanoparticles used for methane catalytic decomposition. *J. Phys. Chem. C* **2012**, *116*, 21577.

(8) Zhu, X.; Cheng, D.; Kuai, P. Catalytic decomposition of methane over Ni/Al_2O_3 catalysts: Effect of plasma treatment on carbon formation. *Energy Fuels* **2008**, *22*, 1480.

(9) Chen, D.; Christensen, K. O.; Ochoa-Fernandez, E.; Yu, Z. X.; Totdal, B.; Latorre, N.; Monzon, A.; Holmen, A. Synthesis of carbon nanofibers: effects of Ni crystal size during methane decomposition. *J. Catal.* **2005**, *229*, 82.

(10) Liu, C. J.; Ye, J. Y.; Jiang, J. J.; Pan, Y. X. Progresses in the preparation of coke resistant ni-based catalyst for steam and CO_2 reforming of methane. *ChemCatChem* **2011**, *3*, 529.

(11) Dehghan-Niri, R.; Walmsley, J. C.; Holmen, A.; Midgley, P. A.; Rytter, E.; Dam, A. H.; Hungria, A. B.; Hernandez-Garrido, J. C.; Chen, D. Nanoconfinement of Ni clusters towards a high sintering resistance of steam methane reforming catalysts. *Catal. Sci. Technol.* **2012**, *2*, 2476.

(12) Takenaka, S.; Kobayashi, S.; Ogihara, H.; Otsuka., K. Ni/SiO_2 catalyst effective for methane decomposition into hydrogen and carbon nanofiber. *J. Catal.* **2003**, *217*, 79.

(13) Martinez-Latorre, L.; Armenise, S.; Garcia-Bordeje, E. Temperature-mediated control of the growth of an entangled carbon nanofiber layer on stainless steel micro-structured reactors. *Carbon* **2010**, *48*, 2047.

(14) Li, J.; Croiset, E.; Ricardez-Sandoval, L. Methane dissociation on Ni(100), Ni(111), and Ni(553): A comparative density functional theory study. *J. Mol. Catal. A-Chem.* **2012**, *365*, 103.

(15) Pan, Y. X.; Liu, C. J.; Shi, P. Preparation and characterization of coke resistant Ni/SiO_2 catalyst for carbon dioxide reforming of methane. *J. Power Sources.* **2008**, *176*, 46.

(16) Zhu, X.; Huo, P.; Zhang, Y. P.; Cheng, D. G.; Liu, C. J. Structure and reactivity of plasma treated Ni/Al_2O_3 catalyst for CO_2 reforming of methane. *Appl. Catal., B* **2008**, *81*, 132.

(17) Shang, S. Y.; Liu, G. H.; Chai, X. Y.; Tao, X. M.; Li, X.; Bai, M. G.; Chu, W.; Dai, X. Y.; Zhao, Y. X.; Yin, Y. X. Research on Ni/gamma-Al_2O_3 catalyst for CO_2 reforming of CH_4 prepared by atmospheric pressure glow discharge plasma jet. *Catal. Today.* **2009**, *148*, 268.

(18) Lay, E.; Metcalfe, C.; Kesler, O. The influence of incorporating MgO into Ni-based cermets by plasma spraying on anode microstructural and chemical stability in dry methane. *J. Power Sources.* **2012**, *218*, 237.

(19) Hua, W.; Jin, L. J.; He, X. F.; Liu, J. H.; Hu, H. Q. Preparation of Ni/MgO catalyst for CO_2 reforming of methane by dielectric-barrier discharge plasma. *Catal. Commun.* **2010**, *11*, 968.

(20) Yan, X.; Liu, Y.; Zhao, B.; Wang, Z.; Wang, Y.; Liu, C. J. Methanation over Ni/SiO_2: Effect of the catalyst preparation methodologies. *Int. J. Hydrogen Energy.* **2013**, *38*, 2283.

(21) Yan, X.; Liu, C. J. Effect of the catalyst structure on the formation of carbon nanotubes over Ni/MgO catalyst. *Diamond Relat. Mater.* **2013**, *31*, 50.

(22) Sun, Q. D.; Yu, B.; Liu, C. J. Characterization of ZnO nanotube fabricated by the plasma decomposition of $Zn(OH)_2$ via dielectric barrier discharge. *Plasma Chem. Plasma Process.* **2012**, *32*, 201.

(23) Ye, J. Y.; Liu, C. J. $Cu_3(BTC)_2$: CO oxidation over MOF based catalysts. *Chem. Commun.* **2011**, *47*, 2167.

(24) Liu, Y.; Pan, Y.; Wang, Z. J.; Kuai, P.; Liu, C. J. Facile and fast template removal from mesoporous MCM-41 molecular sieve using dielectric-barrier discharge plasma. *Catal. Commun.* **2010**, *11*, 551.

(25) Liu, Y.; Pan, Y. X.; Kuai, P.; Liu., C. J. Template removal from ZSM-5 Zeolite using dielectric-barrier discharge plasma. *Catal. Lett.* **2010**, *135*, 241.

(26) Zou, J. J.; Liu, C. J.; Zhang, Y. P. Control of the metal−support interface of NiO-loaded photocatalysts via cold plasma treatment. *Langmuir.* **2006**, *22*, 2334.

(27) Burghgraef, H.; Jansen, A. P. J.; van Santen, R. A. Methane activation and dehydrogenation on nickel and cobalt: A computational study. *Surf. Sci.* **1995**, *324*, 345.

(28) Zhu, X.; Cheng, D.; Kuai, P. Catalytic decomposition of methane over Ni/Al_2O_3 catalysts: Effect of plasma treatment on carbon formation. *Energy Fuels.* **2008**, *22*, 1480.

(29) Park, C.; Keane, M. A. Catalyst support effects in the growth of structured carbon from the decomposition of ethylene over nickel. *J. Catal.* **2004**, *221*, 386.

(30) Hofmann, S.; Csanyi, G.; Ferrari, A. C.; Payne, M. C.; Robertson, J. Surface diffusion: The low activation energy path for nanotube growth. *Phys. Rev. lett.* **2005**, *95*, 036101.

(31) Kroll, V. C. H.; Swaan, H. M.; Mirodatos, C. Methane reforming reaction with carbon dioxide over Ni/SiO_2 Catalyst: I. Deactivation studies. *J. Catal.* **1996**, *161*, 409.